RSC Advances

PAPER

View Article Online
View Journal | View Issue



Cite this: *RSC Adv.*, 2025, **15**, 6357

# Preparation of nanosilver/polymer composites and evaluation of their antimicrobial and antitumor effect

FeiFei Lu,[a] Yuxin Liu,[b] Yingxin Dai,[b] Guoxu Zhang*[b] and Yanan Tong *[b]

In this study, a copolymer (PVA-*g*-PEG) of polyethylene glycol (PEG) and polyvinyl alcohol (PVA) was synthesized by grafting PEG chains onto PVA backbone. PVA-*g*-PEG was used as the carrier to prepare the silver nanoparticles/polymer composite (AgNPs/PVA-*g*-PEG) using a "one-pot" biological method in the presence of grape seeds extract as a reducing and stabilizing agent. In order to highlight the effect of the copolymer, the homo-polymers PVA and PEG were applied as the carriers to prepare the corresponding composites – AgNPs/PVA, and AgNPs/PEG, respectively using the same method. The prepared AgNPs/polymer products were characterized by UV absorption spectroscopy (UV-vis), scanning electron microscopy (SEM) and X-ray diffraction (XRD). The results show that the silver ions were successfully reduced by the grade seeds extract and the produced AgNPs are coated on the surface of AgNPs/PVA-*g*-PEG and AgNPs/PVA, but not for AgNPs/PEG. The prepared AgNPs are uniform and monodisperse, the particle size is small with mean diameter about 25.7 ± 2.3 nm and 54.2 ± 3.4 nm for AgNPs/PVA-*g*-PEG and AgNPs/PVA, respectively. The AgNPs/polymer composites exhibited superior antimicrobial effects against microorganisms (*Escherichia coli* and *Staphylococcus aureus*). AgNPs/PVA-*g*-PEG demonstrated a better performance than AgNPs/PVA. AgNPs/PVA-*g*-PEG had a minimum inhibitory concentration (MIC) of 1.3 μg $mL^{-1}$ and a minimum inhibitory concentration (MBC) of 2.4 μg $mL^{-1}$ against the microorganisms. For anti-tumor effect, AgNPs/PVA-*g*-PEG also demonstrated a high cytotoxicity to the colorectal cancerous cells HCT116 and SW620. The IC50 values of AgNPs/PVA-*g*-PEG for HCT116 and SW620 cell lines were 25.4 and 37.6 μg $mL^{-1}$, respectively, suggesting a good anticancer activity. All above results indicate that AgNPs/PVA-*g*-PEG composites have a significant potential for the control of microorganisms and inhibition of cancer cells.

Received 15th November 2024
Accepted 27th January 2025

DOI: 10.1039/d4ra08108k

rsc.li/rsc-advances



## Introduction

It has been well known that silver and silver ions have bacteriostatic effects, and they can be applied as inorganic bacteriostatic agents to purify water, prevent food deterioration, and treat infectious diseases.[1–4] Recently, with the rapid development of nanotechnology, the unique physicochemical properties and biological characteristics of some conventional materials at the nanoscale have received widespread attention. Silver nanoparticles (AgNPs) exhibited a much better antibacterial performance compared with traditional silver antibacterial agents owning to the small size and surface effects.[5–17] AgNPs possess a series of advantages, such as wide antibacterial spectrum, long-term antibacterial effect, safety, and high efficiency. In addition, the bacteria treated with AgNPs are less likely to develop resistance. Therefore, AgNPs have been considered as a new type of anti-bacterial agent to replace antibiotics in the future. Until now, AgNPs have been widely used in the fields of chemical, textile, ceramic, food, medicine, clinical and other anti-bacterial fields.[3–16]

Generally, the traditional synthesis of AgNPs include physical and chemical methods.[18–39] However, there were many disadvantages in these methods such as expensive equipment, high-energy consumption, and environmental pollution caused by the use of chemical reagents during the synthesis process.[21] Recently, emerging biosynthetic methods have been applied to replace chemical reagents with extracts of biological materials such as plants, bacteria, fungi, and algae, which function as reducing agents and stabilizers, to reduce the highly unstable silver ions to stable AgNPs. Compared with traditional synthetic methods, these new approaches are easy to operate, mild in reaction conditions, low-cost, and environmentally friendly.[23,24] At present, various plant extracts such as lemon, hawthorn, and ginger have been used to synthesize AgNPs.[20,27,30–32,34] However, the final products prepared from various starting biomaterials exhibited different shapes, sizes, and surface bound

[a]*College of Medicine and Biological Information Engineering, Northeastern University, Shenyang, Liaoning, 110167, China*

[b]*Department of Nuclear Medicine, General Hospital of Northern Theater Command, No. 83, Wenhua Road, Shenyang 110016, China. E-mail: Yanan_tong@126.com; zhangguoxu_502@163.com*

biomolecules.[25–27] Most importantly, their anti-bacterial and stability properties also varied significantly. Therefore, screening novel and inexpensive biomaterials becomes a key factor to synthesize highly efficient AgNPs anti-bacterial agents.

Grape seeds contain a lot of crude proteins, amino acids, carbohydrates, vitamins, trace elements, unsaturated fatty acids, as well as polyphenolic compounds such as catechins, epicatechins, gallates, and anthocyanins. Among these substances, anthocyanins account for 80% of the polyphenolic compounds. Hence, grape seed extract has been considered as so far the most efficient antioxidant which was derived from plants.[40,41] However, as a waste of grape and wine processing, grape seeds have not been utilized and they actually possess great potential for development and utilization.

In this study, the grape seed extract was applied as a reducing agent and stabilizer to synthesize AgNPs. A composite nanosilver antibacterial agent was prepared by combining AgNPs with a carrier to further effectively prevent the aggregation and deposition of AgNPs. Polymers are well-known skeleton materials for metal nanoparticles. When nanoparticles are loaded onto the polymer, the polymer backbone acts as a dispersant and protective agent. Polyvinyl alcohol (PVA) is a water-soluble polymer that is safe, non-toxic, highly transparent, easy to process, and has good biocompatibility, biodegradability, thermal stability, and film-forming properties.[42–44] PVA is an ideal carrier and has been widely used in nanocomposites. In addition, the water solubility of PVA makes AgNPs composites easily be prepared in an aqueous solution. Polyethylene glycol (PEG) is a highly biocompatible polymer material commonly used for drug delivery and surface modification of nanomaterials. By modifying with PEG, the dispersibility and stability of nanoparticles in aqueous solutions can be improved, while reducing non-specific interactions between nanoparticles and living organisms. In previous studies, the end of the PEG molecular chain is modified with methoxy ($CH_3O$–), which enhances the stability and biocompatibility of PEGylated AgNPs[45,46] in aqueous solution while maintaining their original properties, including – first, excellent biocompatibility and bio-macromolecular modification: PEG modification enhances the compatibility of AgNPs within living organisms, also facilitating further surface modifications, such as antibodies and peptides, to achieve more accurate biometric recognition and detection. Second, low side effects: PEG modification reduces non-specific interactions between silver nanoparticles and organisms to decrease their potential biological toxicity. Third, easy to modify with specific molecules in the following stage: PEGylated AgNPs have good stability and dispersibility, making them easy to modify with specific molecules in the next stage, such as fixing biomolecules on the surface of nanoparticles through chemical bonding or physical adsorption. In current work, a graft copolymer (PVA-*g*-PEG) of ethylene glycol and vinyl alcohol repeating units was synthesized and used as the carrier to prepare the nanosilver/copolymer composite. The performance of AgNPs prepared from the copolymer was compared with the product from PVA alone. Evaluations were conducted on the anti-bacterial effect against microorganisms (*Escherichia coli* and *Staphylococcus aureus*) and anti-tumor activity against HCT116 and SW620 Cells. The study is highly important to the development and application of nanosilver-based anti-bacterial and anti-tumor agents.[47]

## Materials and methods

### Materials

PVA (90.0% hydrolyzed, molecular weight 63 000 g $mol^{-1}$, polydispersity index 2.07) was purchased from Innochem (Beijing, China). The grape seed extract with an extract ratio of 10 : 1 was purchased from Beijing Psaitong Biotechnology Co., Ltd (Beijing, China). Poly(ethylene glycol) methyl ether (PEGME, molecular weight 2000 g $mol^{-1}$, polydispersity index 1.10), *p*-toluenesulfonyl chloride (TsCl), triethylamine, sodium hydride (NaH, 60% dispersed in mineral oil), silver nitrate ($AgNO_3$), dimethyl sulfoxide (DMSO), dichloromethane, diethyl ether and other chemicals were purchased from Sigma-Aldrich and used as received without further purification.

### Synthesis of nanosilver/polymer composite

The grape seed extract was prepared in ultra-pure water. Grape seed sample (5 g) was added into 100 mL ultra-pure water, the mixture was heated and refluxed at 90 °C for 1 hour. After cooling to room temperature, the mixture was centrifuged at 5000 rpm for 20 minutes. The yellow brown supernatant was stored in a fridge at 4 °C. The polymer (0.5 g) and $AgNO_3$ (0.05 g) were dissolved into 200 mL ultra-pure water in a round bottom flask which was immersed in a water bath. After stirring for 20 minutes, grape seed extract fluid (5 mL) was added and refluxed at 90 °C for 30 minutes. The mixture was stored in dark at 4 °C. As a control sample, the AgNPs product without any polymers was synthesized from grape seed extract according to above procedures.

### Characterization methods

$^1$H NMR spectra were acquired with a 400 MHz NMR spectrometer (JEOL JNM-ECS) at ambient temperature using deuterated solvent DMSO-$d_6$.

UV-vis absorption spectra of various solution were obtained using a UV-vis spectrophotometer (U-5100 model, Hitachi, Japan) with wavelength scanning range of 300–800 nm. The polymer and grape seed extract samples were used as controls.

The morphology and particle size of synthesized AgNPs particles were characterized using Scanning Electron Microscopy (SEM) (Hitachi SU8000) at 25 °C. The sample solutions were frozen using liquid nitrogen, then made electrically conductive by coating, in a vacuum with a thin layer of gold (approximately 300 Å) for 30 s and at 30 W. The SEM images were taken at an excitation voltage of 10 kV.

The crystal structure of AgNPs/polymer composite was analyzed using an X-ray diffraction (XRD) analyzer (XRD-7000 model, Shimadzu Corporation, Japan) with Cu K$\alpha$ radiation in a 2$\theta$ range of 5–90°. The surface micro-morphology was identified using a field-emission scanning electron microscope

(model S-4800, Hitachi Co., Tokyo, Japan), equipped with X-ray energy dispersive spectroscopy capabilities. X-ray photoelectron spectra were recorded on a spectrometer (Thermo Fisher ESCALAB 250Xi).

### Antimicrobial zone experiment

The cup method was applied to detect the antimicrobial activity of AgNPs/polymer against two microorganisms *Escherichia coli* and *Staphylococcus aureus*. The microorganisms were inoculated into 2216E culture medium and cultured at 26 °C with 150 rpm until the logarithmic growth stage, physiological saline was used to dilute to $10^6$ CFU $mL^{-1}$ 100 μL of each sample was taken and evenly spread onto 2216E solid culture medium plates. Four Oxford cups (inner diameter 6 mm, outer diameter 8 mm) were placed evenly on each plate. 20 μL of AgNPs/polymer complex synthesized from grape seed exact was added into the Oxford cups. Similarly, the AgNPs sample without polymer was treated using the same methods and used as the control. All samples were loaded in an incubator at a constant temperature of 26 °C for 24 hours. The diameter of the inhibition zone of each microorganism was measured and the experiment was repeated for three time. The final results were expressed by the average diameter of the inhibition zone ± standard deviation (SD).

### Determination of minimum inhibitory concentration (MIC) and minimum bactericidal concentration (MBC)

*E. coli* was used as an indicator bacterium, the solution was diluted to $10^6$ CFU $mL^{-1}$ and cultured to the logarithmic growth stage. The synthesized AgNPs/polymer solution was diluted into different concentration gradients using the double dilution method,[44] 1 mL of AgNPs/polymer solution at various concentrations was sequentially added to the test tubes containing bacterial solution and they were mixed well. Two control tubes were established with a negative control of 2 mL 2216E liquid culture medium and a positive control of 2 mL $10^6$ CFU per mL bacterial suspension, respectively. After shaking at 26 °C for 24 hours, growth of the bacterial cells was visually observed. Negative (−) mark was recorded if the mixture in the test tube is clear. On the opposite, positive (+) mark was recorded if the mixture in the test tube is turbid. The lowest concentration of AgNPs/polymer solution in the negative testing tube corresponds to the MIC of AgNPs/polymer. 100 μL of the solution from the negative testing tube was taken and transferred onto a 2216E solid culture medium plate. The plate was inverted for 24 hours at 26 °C to observe and record the growth of the colonies. The culture dish with less than five growing colonies was marked negative (−), otherwise the culture dish was marked positive (+). The lowest concentration of AgNPs/polymer on the negative plate was defined as the MBC of AgNPs/polymer. All above experiments were repeated three times for average values and standard deviations.

### Antimicrobial kinetics

The indicator bacterium *E. coli* was cultured in 2216E liquid medium at 26 °C and 150 rpm until reached the logarithmic growth stage, then it was diluted to $10^6$ CFU $mL^{-1}$. According to the experimental results of MIC and MBC, AgNPs/polymer at final concentrations of 1 μg $mL^{-1}$ and 2 μg $mL^{-1}$ were added to the bacterial solution for treatment. The bacterial solution with physiological saline was used as a control and incubated at a constant temperature of 26 °C on a shaker at 150 rpm. Samples were taken at the time of 0, 10, 30, 60, 120, and 180 minutes, and the absorbance at 600 nm was measured the UV-vis spectrophotometer to plot the antibacterial kinetics curve. All above experiment was repeated for three times.

### Nucleic acid release

The nucleic acid in the released cytoplasm due to damage of the bacterial cell membrane can be detected by measuring the absorbance at 260 nm. The experimental procedures are given below: the indicator bacterium *E. coli* in logarithmic stage was diluted to $10^6$ CFU $mL^{-1}$, AgNPs/polymer was added to adjust the final concentrations at 1 and 2 μg $mL^{-1}$, physiological saline was used as the control group to culture for 3 hours at 26 °C. The bacterial samples were taken at fixed time intervals and centrifuged using 5000 rpm for 20 minutes. The absorbance $A_{260}$ of the supernatant at 260 nm was determined using the UV-vis spectrophotometer to evaluate the effect of AgNPs/polymer on cell content release.[48] All above experiment was repeated for three times.

### Cell culture

The cell lines for colorectal cancer cells HCT116 and SW620 were cultured to generate a cell bank to place the cell lines in ELISA kits. The cell line was maintained using 500 ML Dulbecco's Modified Eagle's Medium (DMEM) (Sigma-Aldrich) containing high concentrations of phosphate buffer, L-glutamine and 2-[4-(2-hydroxyethyl)piperazin-1-yl]ethanesulfonic acid (HEPES). For the medium of cell growth, 100 mL of DMEM was used which contains 15% fetal bovine serum, filtrate, and 1% antibiotics. Cell culture was conducted in an incubator at 37 °C.

### IC50 determination

The AgNP solutions were prepared using 100 mL DMEM in a fridge. The culture medium in the ELISA kit was transferred using a Pasteur pipette, which was connected with a Buchner funnel under vacuum. The cells adhered at the bottom of the box where remained untouched during the experiment. The well were rinsed by 100 μL PBS and extracted using a Pasteur pipette. AgNP solutions were introduced to contact with the cells for 24 hours at 37 °C under a $CO_2$ atmosphere. AgNPs were dissolved into the growth medium by formation of suspensions. This test was conducted with the AgNPs prepared by PVA-*g*-PEG, PVA, and PEG, respectively.

### MTT cell viability investigation

The cytotoxicity of the AgNPs prepared from PVA-*g*-PEG, PVA, and PEG in cancer cell lines and normal cell lines was investigated using MTT assay, which was used to determine the cell

viability rate by a colorimetric method according to the amount of formazan generated from the living cells. The measurement was conducted by three stages. First, the culture medium and AgNPs were remove with a Pasteur pipette after 24 hours; second, 200 μL of growth medium and 20 μL of MTT were dissolved into 200 μL DMSO at a PBS concentration of 5 mg per mL PBS, the mixture was added to each well along with the uncleaned cells, then it was incubated at 37 °C under a $CO_2$ atmosphere for 6 hours to synthesize formazan, third, the supernatant was loaded into a new ELISA kit and a UV-vis analysis was conducted at a wavelength of 595 nm for each plate (Varioskan LUX).

### Data analysis

The obtained data were analyzed to calculate the mortality rate and to compare the concentration of formazan in treated cells with that in the untreated cells (0% mortality) at each concentration of AgNPs. The mortality rates were plotted as a function of AgNPs concentration in a log scale. IC50 results were calculated using the four parameter logistic (4PL) regression,[18] which was commonly used model for analysis of biological determination. A linear relationship is usually yielded within specific range of concentration. An equation that describing regression is given below

$$f(x) = a + \frac{b-a}{1+\left(\frac{x}{c}\right)^d} \quad (1)$$

where $f(x)$ represents the mortality as a function of AgNPs concentration ($x$), four parameters are the minimum mortality rate at zero concentration ($a$), the maximum mortality rate at infinite concentration ($b$), the inflection point ($c$), and the Hill slope of the curve ($d$). The parameter $d$ and IC50 represent the concentration at which the mortality reaches the inflection point. IC50 was determined from the inflection point of the curve. To ensure if significant statistical differences were present for each sample and between the samples, ANOVA was used to analyze the data with a $p < 0.05$ representing that the data were not significant.

## Results and discussion

### Synthesis of the graft copolymer

The schemes in Fig. 1 describe the synthesis protocol that was followed to prepare the PVA-*g*-PEG product. First, the hydroxyl ends of the PEGME were reacted with TsCl to yield PEGME-Ts. In a second step, excess of PEGME-Ts was reacted with deprotonated PVA to remove the toluenesulfonyl group of PEGME-Ts and graft the PEG chains onto PVA backbone to yield the PVA-*g*-PEG copolymer. The detailed synthesis procedures is described below.

Synthesis of PEGME-Ts is shown in Fig. 1A. In a round-bottom flask, PEGME was dissolved into freshly distilled dichloromethane. Nitrogen was introduced to keep the solution maintain a $N_2$ atmosphere. Three-fold excess (in mole) of triethylamine was added to the solution after PEGME was fully dissolved. The flask was immersed in an ice bath and the

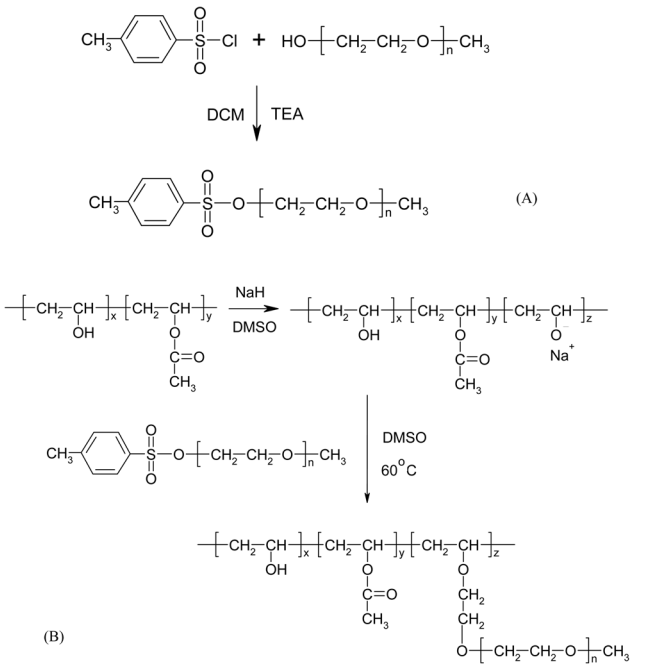


Fig. 1 Synthesis of PEGME-Ts (A) and PVA-*g*-PEG (B).

solution was stirred for around 20 min. Three-fold excess (in mole) of TsCl was added in a small quantity during 5–10 minutes. After half an hour, the ice bath was removed and the reaction was kept at room temperature. After stirring for overnight, the solution was concentrated under vacuum and added dropwise to a large amount of diethyl ether. The white precipitate (PEGME-Ts) was filtrated and dried in a vacuum oven at room temperature for overnight. The dry PEGME-Ts was ground into powder, suspended in toluene and stirred for 1 h. The impurities, including excess trimethylamine, TsCl, and by-product trimethylamine hydrochloride, were filtered off and the filtrate was concentrated again and added dropwise to diethyl ether. The white precipitate was collected by filtration and dried for overnight under vacuum.

Unmodified PEGME (Fig. 2A). $^1$H NMR (DMSO-$d_6$), $\delta$ (ppm): 4.5 (t, ~1H, –OH), 3.2–3.7 (massive peaks, –O–$CH_2$–$CH_2$– from PEG backbone), 3.2(~3H, –$CH_3$).

PEGME-Ts (Fig. 2B). $^1$H NMR (DMSO-$d_6$), $\delta$ (ppm): 7.4 (d, ~2H, benzyl ring), 7.7 (d, ~2H, benzyl ring), 4.1 (t, ~2H, –$CH_2$–), 3.2–3.7 (massive peaks, –O–$CH_2$–$CH_2$– from PEG backbone), 3.2(~3H, –$CH_3$).

As shown in Fig. 1A, PEGME exhibits a triplet for the terminal hydroxyl group at around 4.5 ppm in DMSO-$d_6$ and this peak does not shift or broaden with the concentration of the polymer, water, or impurities and is well separated from the main chemical shift of the PEGME backbone.[49,50] Therefore, DMSO-$d_6$ was used as the NMR solvent to investigate the functionality of PEGME. The disappearance of this peak suggests that all PEGME chains have been successfully modified with the tosylate groups. Furthermore, the peak at 4.1 ppm represents two protons of the last ethylene glycol unit next to the tosylate

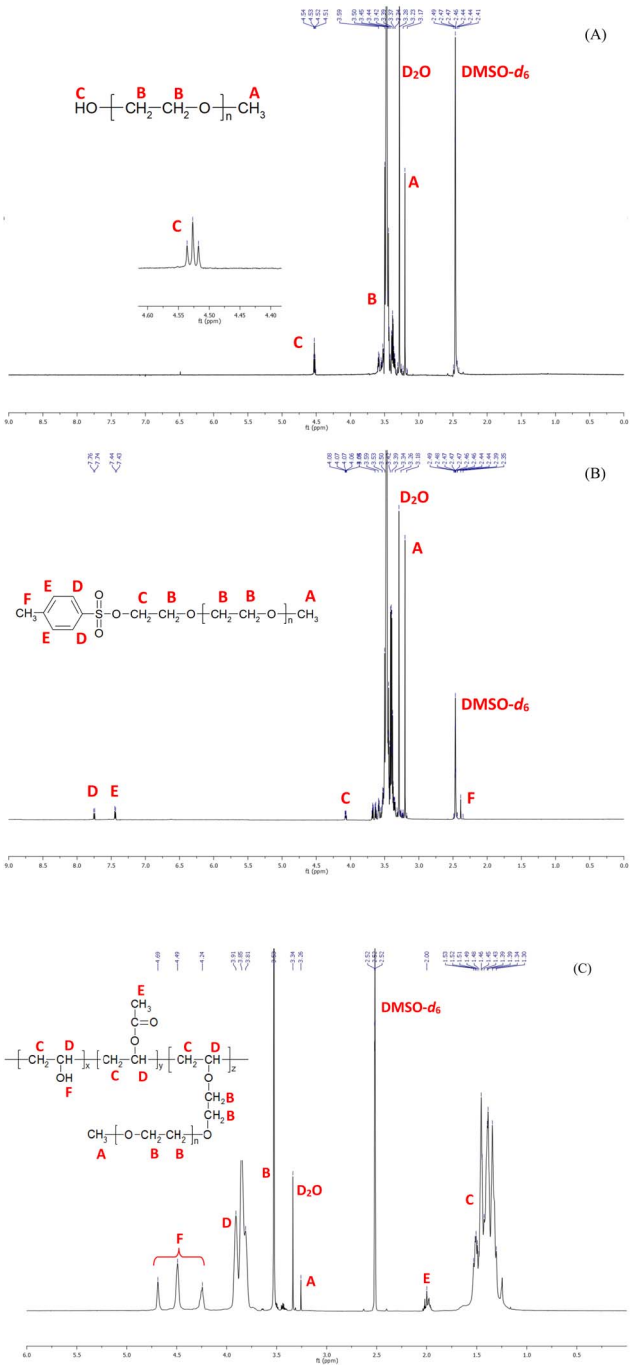


Fig. 2 $^{1}$H NMR spectra of PEGME (A), PEGME-Ts (B), and PVA-*g*-PEG (C).

group, again indicating that the tosylate group was covalently attached at the PEGME chain end.

Synthesis of PVA-*g*-PEG is shown in Fig. 1B PVA was dissolved into freshly distilled DMSO in a round-bottom flask. Nitrogen was introduced to keep the solution maintain a $N_2$ atmosphere. A certain amount of NaH was added and the mixture was stirred at room temperature for 1 h. PEGME-Ts was added to the reaction flask which was then placed in an oil bath at 60 °C and stirred overnight under nitrogen. The oil bath was removed and the mixture was cooled down to room temperature after quenching the reaction with a drop of water. The solution was concentrated and precipitated into diethyl ether, the solid PVA-*g*-PEG was collected from filtration and dried at room temperature under vacuum for 12 h.

To purify the final product, PVA-*g*-PEG was dissolved in deionized (DI) water and dialyzed against a large amount of DI water using a dialysis bag with a cut-off molecular weight of 7000 g mol$^{-1}$ for one week. The concentrated solution was freeze dried and precipitated in diethyl ether. After the final precipitation, the solid was dried at room temperature under vacuum for 2 days. The disappearance of the peaks at 4.5 and 4.1 ppm suggests that all PEG chains were successfully grafted onto PVA backbone.

PVA-*g*-PEG. $^{1}$H NMR (DMSO-$d_6$), $\delta$ (ppm): 4.0–5.0 (t, ~1H, –OH), 3.8–3.9 (multiple peaks, –CH– from PVA main chain), 3.2–3.7 (massive peaks, –O–$CH_2$–$CH_2$– from grafted PEG backbone), 3.2(~3H, –$CH_3$ of PEG methyl group), 2.0 (t, ~3H, –$CH_3$ at PVA main chain), 1.3–1.5 (multiple peaks, –$CH_2$– from PVA main chain).

## UV-vis spectroscopy

Under the irradiation using visible light, the conduction electrons of metal nanoparticles were excited to generate surface plasmon resonance (SPR), which produces very strong absorption peaks and the bulk indicate colors with wavelength in the region of visible light. The absorption peak of SPR of typical AgNPs is located in the range between 400 and 500 nm.[51] Due to the difference in concentration and particle size, AgNPs solutions exhibit characteristic colors ranging from golden yellow to brown.[52] The polymer solutions are colorless and transparent, and the color of the grape seed extract is slightly yellow. After the heating reaction for 30 minutes, the reaction solution changed from light yellow to deep brown, indicating that $AgNO_3$ was rapidly reduced to AgNPs under the combined action from unsaturated fatty acids, catechins, and anthocyanins in grape

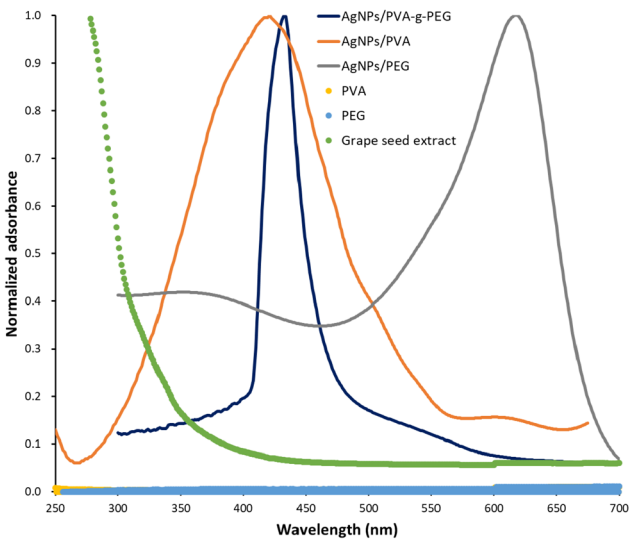


Fig. 3 UV-vis spectra of the AgNPs prepared from different polymers.

seed extract. The absorption spectra of AgNPs/PVA-*g*-PEG was acquired by UV-vis spectrophotometer. The results shown in Fig. 3 indicate that the absorption of AgNPs/PVA-*g*-PEG and AgNPs/PVA solutions exhibits a clear characteristic peak at around 433 and 421 nm, respectively. While AgNPs/PEG solution shows an absorbance peak at 619 nm, and grape seed extract and the polymer solutions did not exhibit any peaks within the wavelength scanning region, further confirming the preparation of AgNPs/PVA-*g*-PEG and AgNPs/PVA. It has been found that the AgNPs with a narrow absorption peak have a more uniform particle size distribution. Therefore, AgNPs/PVA-*g*-PEG should be more uniformly distributed comparing that of AgNPs/PVA, as the absorption peak is narrow with AgNPs/PVA-*g*-PEG. For AgNPs/PEG, maybe the profiles of the NPs are quite different with AgNPs/PVA-*g*-PEG and AgNPs/PVA, or the AgNPs/PEG aggregate to give an absorbance peak at 619 nm from the UV-vis spectra.

### Morphology and particle size analysis

The particle size and morphology of AgNPs/polymer were detected using SEM. Fig. 4 shows the morphological observation, particle size distribution, and X-ray diffraction patterns of the prepared AgNPs/polymer samples. The SEM images show that AgNPs/PVA-*g*-PEG and AgNPs/PVA are spherical and well dispersed with a relatively homogeneous particle size, while AgNPs/PEG seem to be less dispersed and aggregate to form bulk with a large scale. The statistical analysis of particle size distribution (Fig. 4D) shows that the particle size range of AgNPs/PVA-*g*-PEG is between 5–50 nm, with an average particle size of 25.7 ± 2.3 nm. For AgNPs/PVA, Fig. 4E indicates that the particle size distribution ranges from 10 to 80 nm, with an average diameter of 54.2 ± 3.4 nm. To both synthesized particle AgNPs/PVA-*g*-PEG and AgNPs/PVA, their size follows a normal distribution, and the size distribution is relatively concentrated. However, the size distribution of AgNPs/PEG cannot be acquired due to formation of large aggregates. Comparatively, AgNPs/PVA-*g*-PEG particles are well dispersed on the polymeric carriers without obvious agglomeration, while AgNPs/PVA exhibits slight tendency for particle agglomeration. The observed phenomenon could be attributed to the protective effect of PEG chain. PVA has been known to be a good carrier for nanoparticles to prepare nanocomposites. In this study, after the silver nanoparticles bound to PVA chains, the hydrophilic PEG grafts covered the nanocomposites to stabilize them.[22] Thus, AgNPs/PVA-*g*-PEG shows excellent dispersive properties. The mechanisms are illustrated in Fig. 5. Previous studies have indicated that the AgNPs with a smaller size possess a higher anti-bacterial activity.[53] However,

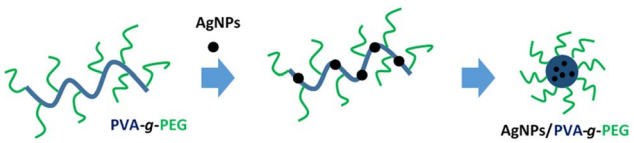


Fig. 5 Mechanisms of dispersive AgNPs/PVA-*g*-PEG.

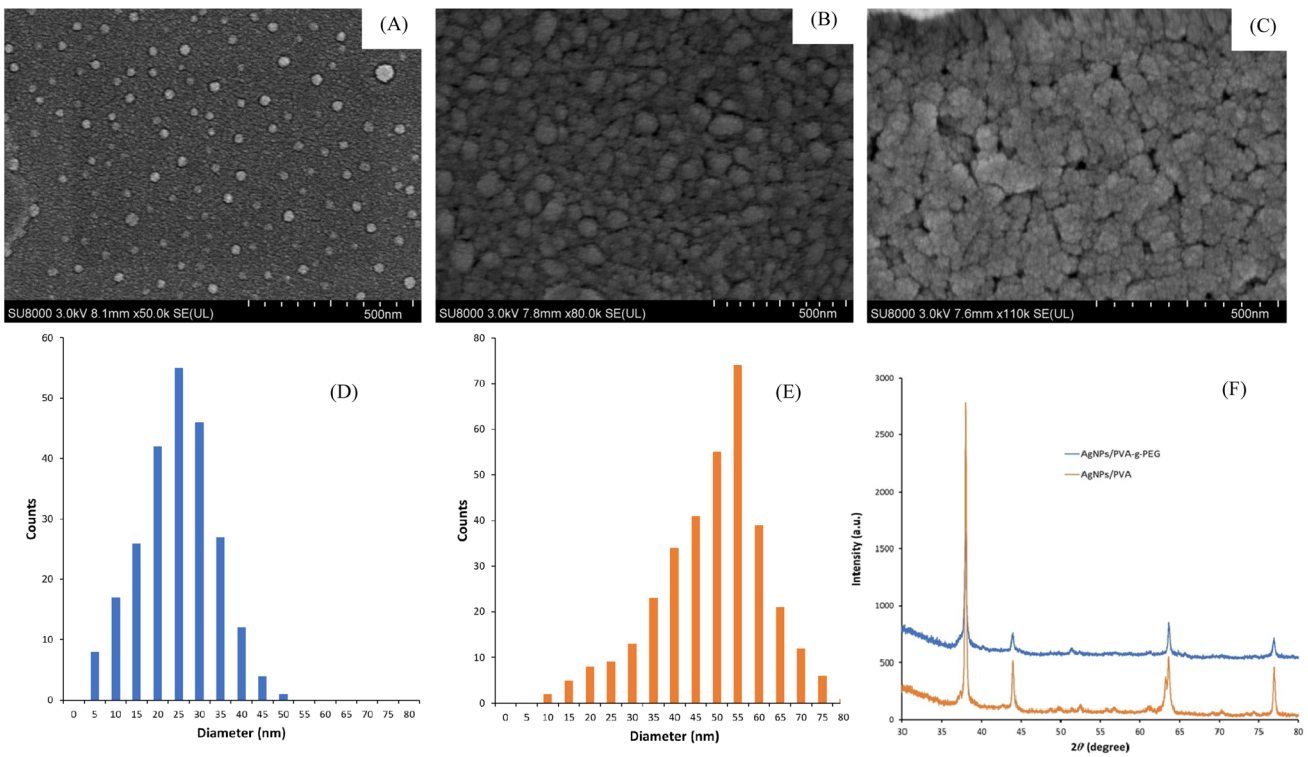


Fig. 4 SEM images of AgNPs/PVA-*g*-PEG (A), AgNPs/PVA (B), and AgNPs/PEG (C). Size distribution of AgNPs/PVA-*g*-PEG (D), AgNPs/PVA (E). X-ray diffraction patterns of AgNPs/PVA-*g*-PEG and AgNPs/PVA (F).

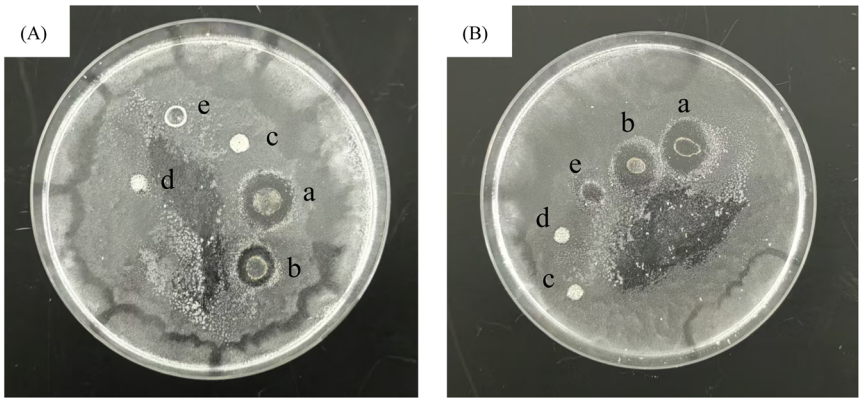


Fig. 6 Antimicrobial effects using the agar diffusion method for *E. coli* (A) and *S. aureus* (B), where (a) AgNPs/PVA-*g*-PEG, (b) AgNPs/PVA, (c) AgNPs/PEG, (d) grape seeds extract, and (e) normal saline.

when the concentration of AgNPs is high or the particle size is less than 40 nm, agglomeration and precipitation might occur due to high surface energy of nano-scale silver particles.[17,18] The aggregation and sedimentation between the AgNPs prepared by biosynthetic method were significantly hindered by the protection and stability of the active ingredients, biomolecules, and functional groups bound to the surface of AgNPs,[54] resulting in an excellent dispersion of AgNPs/polymer particles. In addition, the introduction a polymeric dispersant protective agent such as PVA into the reaction system make the AgNPs particles inserted or encapsulated in the polymer coil, effectively preventing the aggregation of AgNPs and further improving the stability of the final product.[55] Therefore, the grape seed extract and PEG polymeric chains can synergistically enhance the stability of AgNPs.

### Crystal structure analysis

The crystal structures of synthesized AgNPs/PVA-*g*-PEG and AgNPs/PVA were characterized using XRD (Fig. 4F). The results showed that the XRD patterns exhibited four significant diffraction peaks at 2$\theta$ angles of 38.06°, 44.18°, 64.56°, and 77.22°, respectively, which correspond to the (111), (200), (220), and (311) crystal planes of the silver crystal system, indicating that both AgNPs/polymer composites exhibit a face centered cubic (FCC) crystal structure. The average grain size of AgNPs can be obtained from the full width at half maximum of the strongest diffraction peak (111) using Scherrer's formula[56] expressed by eqn (2).

$$D = \frac{k\lambda}{\beta \cos \theta} \quad (2)$$

where $D$ is the average particle size of the sample; $\beta$ is the full width at half maximum of the strongest diffraction peak; $k$ is the Scherrer constant which equals 0.89; $\lambda$ is the X-ray diffraction wavelength of 1.541 nm, and $\theta$ is the diffraction angle. The results calculated from eqn (2) indicate that the average particle size of AgNPs/PVA-*g*-PEG and AgNPs/PVA is 26.3 and 56.1 nm, respectively, which are close to the average particle sizes estimated from SEM.

### Antimicrobial evaluation

The antimicrobial effect of three AgNPs/polymer composites on two microorganisms *E. coli* and *S. aureus* were detected by agar diffusion test, and the results were compared with the grape seeds extract and normal saline. Fig. 6 shows that the grape seed extract and physiological saline in the control groups as well as the AgNPs/PEG group did not display inhibition zones or exhibit antimicrobial activity against the microorganisms. While AgNPs/PVA-*g*-PEG and AgNPs/PVA synthesized from grape seeds showed significant inhibition zones against the microorganisms, indicating that AgNPs/PVA-*g*-PEG and AgNPs/PVA antimicrobial agents have broad-spectrum bactericidal effect. The statistical results of the inhibition zone diameter for the microorganisms are listed in Table 1. Fig. 6 and Table 1 indicate that the diameter of the inhibition zone produced by nanosilver antimicrobial agents varies for different microorganisms, reflecting different sensitivities of the microorganisms to antimicrobial agents. Additionally, the anti-bacterial zone of AgNPs/PVA-*g*-PEG is significantly larger than that of AgNPs/PVA, indicating a stronger antimicrobial activity of the graft copolymer. These results demonstrate that AgNPs/PEG have a high

Table 1 Zone of inhibition of *E. coli* and *S. aureus* with AgNPs/polymer experimental groups and control groups

| | Zone of inhibition (mm) | | | | |
|---|---|---|---|---|---|
| Microorganisms | AgNPs/PVA-*g*-PEG | AgNPs/PVA | AgNPs/PEG | Grape seeds extract | Normal saline |
| *E. coli* | 17.7 ± 0.3 | 15.9 ± 0.7 | 0 | 0 | 0 |
| *S. aureus* | 15.4 ± 0.2 | 13.2 ± 0.6 | 0 | 0 | 0 |

Table 2 MIC and MBC tests of AgNPs/PVA-*g*-PEG composite against *E. coli*

| Label | Concentration (μg mL$^{-1}$) | 24 h | 48 h |
|---|---|---|---|
| 1 | 137.5 | – | – |
| 2 | 68.8 | – | – |
| 3 | 34.4 | – | – |
| 4 | 17.2 | – | – |
| 5 | 8.6 | – | – |
| 6 | 4.3 | – | – |
| 7 | 2.3 | – | – |
| 8 | 1.2 | – | + |
| 9 | 0.6 | + | + |
| 10 | 0.3 | + | + |
| Negative control | | – | – |
| Positive control | | + | + |

surface activity so that they are easily oxidized, aggregated, and precipitated, which reduces the antimicrobial activity and inevitably affects the practical applications of AgNPs.[57] Preparation of AgNPs/PVA-*g*-PEG composite material resulted in the steric hindrance effect of PVA-*g*-PEG on the surface of AgNPs particles, preventing the aggregation of AgNPs and thus improving the antimicrobial effect. Table 1 also shows that the indicator *E. coli* is most sensitive to AgNPs/polymer, which exhibited the largest inhibition zone diameter. Therefore, *E. coli* was used as an indicator bacterium in subsequent inhibition experiments.

### MIC and MBC determination

Using *E. coli* as an indicator, the MIC and MBC of AgNPs/PVA-*g*-PEG (Table 2) and AgNPs/PVA (Table 3) synthesized from grape seeds were determined using double dilution method. Table 2 shows that the bacterial solution in tubes 1–8 is clear, while it becomes turbid after tube 9. Therefore, the critical concentration (1.2 μg mL$^{-1}$) of AgNPs/PVA-*g*-PEG in tube 8 is considered as the MIC of AgNPs/PVA-*g*-PEG. 0.1 mL of bacterial suspension from each tube of 1–8 was taken and loaded onto 2216E solid culture medium. After culturing for 24 hours, growth of

Table 3 MIC and MBC tests of AgNPs/PVA composite against *E. coli*

| Label | Concentration (μg mL$^{-1}$) | 24 h | 48 h |
|---|---|---|---|
| 1 | 65.5 | – | – |
| 2 | 32.8 | – | – |
| 3 | 16.4 | – | – |
| 4 | 8.2 | – | – |
| 5 | 4.1 | – | – |
| 6 | 2.1 | – | – |
| 7 | 1.1 | – | + |
| 8 | 0.5 | + | + |
| 9 | 0.2 | + | + |
| 10 | 0.1 | + | + |
| Negative control | | – | – |
| Positive control | | + | + |

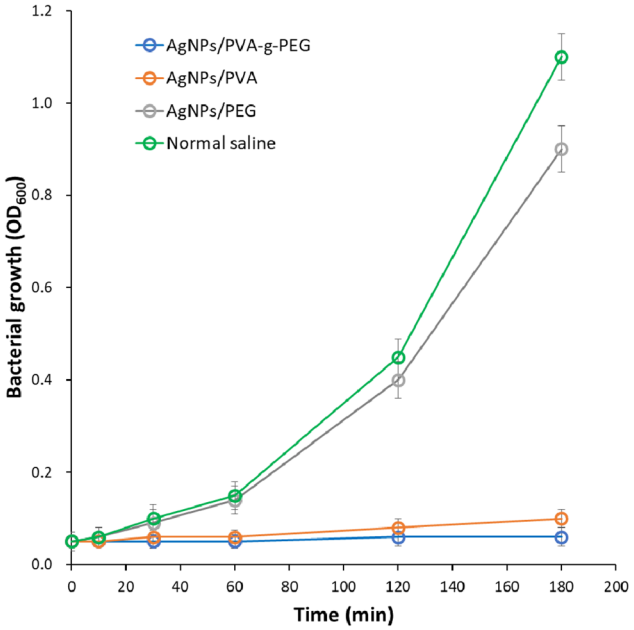


Fig. 7 Growth of *E. coli* treated with different AgNPs.

colonies was observed. It showed that when the concentration of AgNPs/PVA-*g*-PEG reaches 2.3 μg mL$^{-1}$, the indicator hardly generated colonies on the agar plate and was completely killed. Therefore, the MBC of AgNPs/PVA-*g*-PEG for indicator was determined to be 2.3 μg mL$^{-1}$. Table 3 shows that the AgNPs/PVA prepared from grape seeds became cloudy in tube 8. Therefore, the MIC was determined to be 1.1 μg mL$^{-1}$ which corresponds to tube 7, and the MBC was 2.1 μg mL$^{-1}$ which corresponds to tube 6. Because PVA-*g*-PEG is a copolymer, its MIC cannot be directly compared with that of AgNPs/PVA. In the

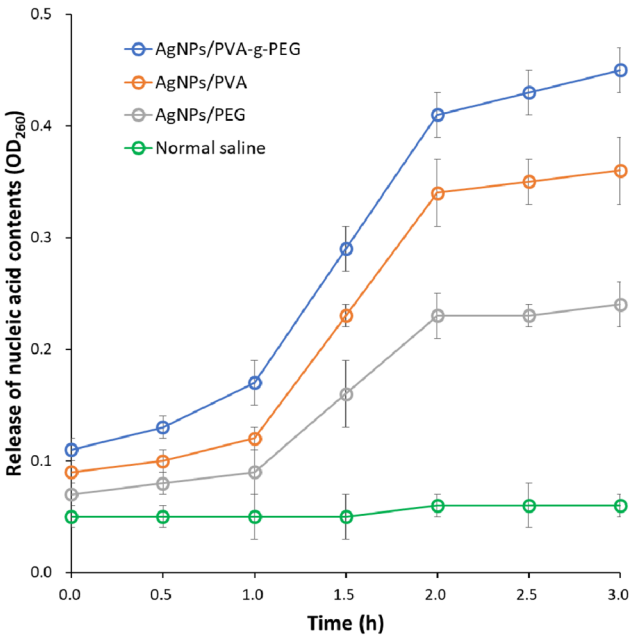


Fig. 8 Effects of different AgNPs on the release of nucleic acid contents from *E. coli*.

synthesis stage, $AgNO_3$ at same concentration and reduction conditions were used to synthesize the two substances, resulting in a same amount of AgNPs in the original solution and various solutions at gradient concentration after dilution. Comparing the data listed in Tables 2 and 3, it can be found that the growth of AgNPs/PVA was observed from the tube #7, while AgNPs/PVA-*g*-PEG started to become cloudy from the tube #8, suggesting that AgNPs/PVA-*g*-PEG has a stronger antimicrobial effect, which is consistent with the results acquired from the inhibition zone test.

### Antimicrobial kinetics

The growth curves of *E. coli* in the presence of synthesized AgNPs/polymer are shown in Fig. 7. The optical density (OD) value of bacterial solution at 600 nm can be applied to reflect the growth of microorganism. Generally, the concentration of microorganism is higher at a higher OD600 value. The control group added with physiological saline shows a continuous increase in OD600 value with increasing culture time, and the bacteria rapidly reached the logarithmic growth stage, exhibiting a typical profile for exponential growth.[53] However, the indicator treated with AgNPs/PVA-*g*-PEG and AgNPs/PVA showed significant inhibitory effects on the indicator. As an increasing cultivation time, OD600 value of the bacterial solutions in both treatment groups remained unchanged. Interestingly, AgNPs/PEG also exhibits a continuous increase in OD600 value with increasing culture time, which is similar to the control group with a logarithmic growth stage, suggesting that the synthesized AgNPs/PEG does not have an effective inhibitory function on the indicator. These results and observation indicate that AgNPs/PVA-*g*-PEG and AgNPs/PVA synthesized

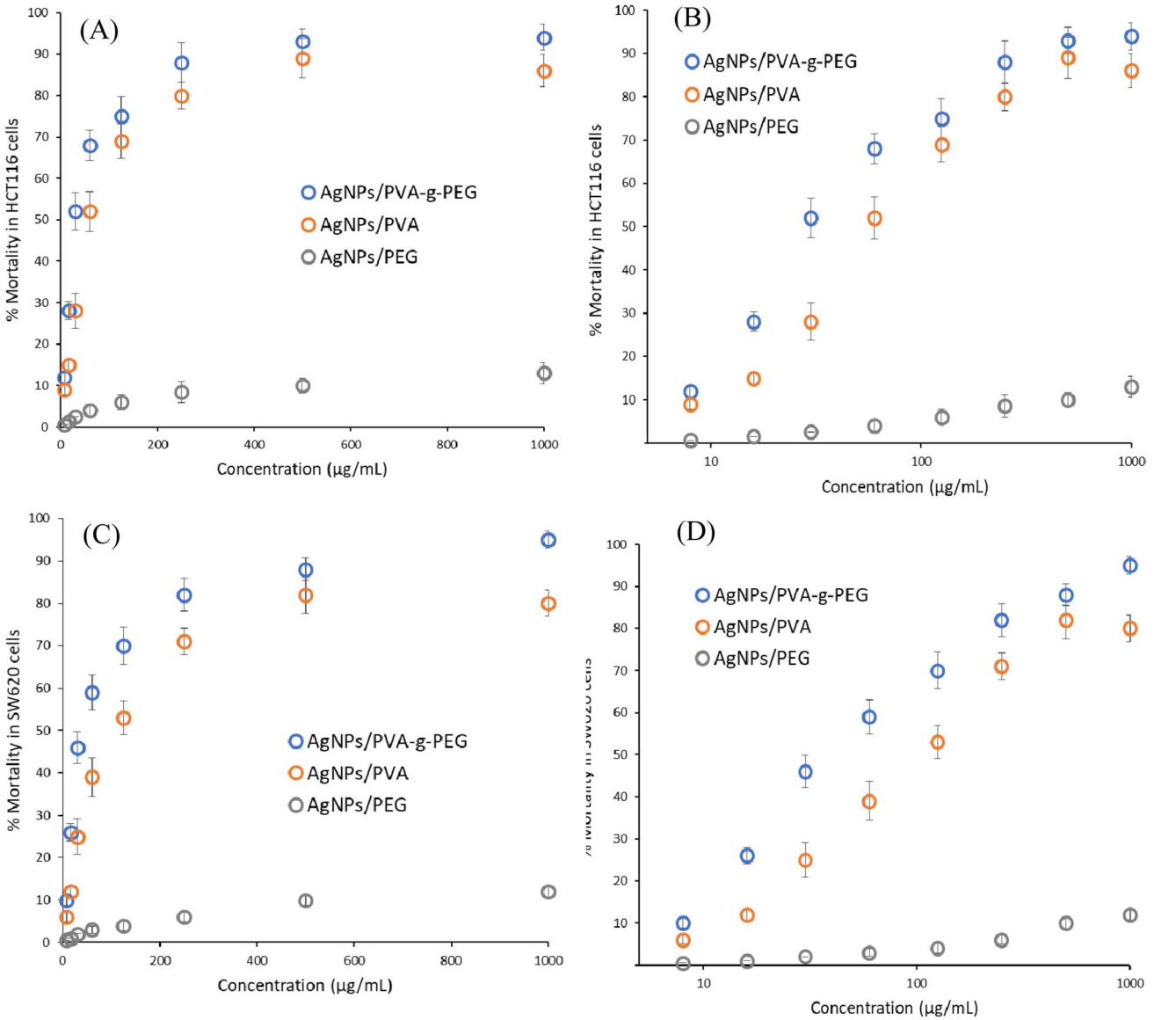


Fig. 9 Cytotoxicity of the AgNPs in HCT116 cells (A and B) and in SW620 cells (C and D) after 24 hours incubation. Log scale and dash lines was applied for fitting of data.

Table 4 IC50 Calculated from 4PL regression method for AgNPs/polymer composites in different cell lines

| Cell line | AgNPs/PVA-*g*-PEG ($\mu g\ mL^{-1}$) | AgNPs/PVA ($\mu g\ mL^{-1}$) | AgNPs/PEG ($\mu g\ mL^{-1}$) |
|---|---|---|---|
| HCT116 | 25.42 ± 1.38 | 51.15 ± 3.66 | 864.23 ± 5% |
| SW620 | 37.64 ± 2.07 | 73.22 ± 4.87 | 1754.36 ± 5% |

from grape seeds have a good inhibitory effect on *E. coli* in an aqueous environment, contributing to the development of nano-silver aquatic antibacterial agents.

### Leakage of cell content

Previous studies have shown that AgNPs adsorbed onto the surface of bacterial cells to disrupt cell membranes and increase cell permeability. Some small molecules such as sodium salts, potassium salts, and phosphates escaped from the cell membranes, followed by some large molecules such as reducing sugars, proteins, and nucleic acids. Such leakage of cell contents disrupted the homeostasis of the intracellular environment and affected the normal function of cellular life activities. As a consequence, the bacterial growth was inhibited, even leading to the death of bacterial.[58,59] Due to the strong UV absorption of nucleic acids at 260 nm, the integrity of the cell membrane can be indicated by detecting the absorbance (OD260) of the bacterial solution at a wavelength of 260 nm. Fig. 8 shows the effect of different AgNPs/polymer on the leakage of contents from indicator cells. It can be seen that the addition of AgNPs/polymer can cause leakage of the contents of *E. coli* cells, and the absorption value of the supernatant at 260 nm increases with increasing treatment time. After treating the bacterial suspension with AgNPs/polymer for 1–2 hours, the corresponding absorbance values rapidly increased by above 50%. Afterwards, the change in OD260 value tended to be stable. While OD260 of the control group supernatant treated with physiological saline remained basically unchanged, indicating that its cell membrane was intact and there was no release of nucleic acids.[60] Among three AgNPs/polymer samples, it can be found that AgNPs/PVA-*g*-PEG showed the most pronounced increase in OD260, followed by AgNPs/PVA, and AgNPs/PEG exhibited the lowest increase in OD260. These results suggest that the AgNPs/polymer especially AgNPs/PVA-*g*-PEG can effectively disrupt the integrity of bacterial cell membranes, thus affecting their normal growth.

### Antitumor effect

The percentage of mortality obtained from MTT assays of each cell line was plotted as a function of AgNPs concentration, the results were shown in Fig. 9. The 4PL regression method was used to fit the curves and to acquire the IC50 values of each bioassay. The fitted curves are shown in Fig. 9 and calculated IC50 results are listed in Table 4.

MTT assays for the AgNPs prepared by PVA-*g*-PEG, PVA, and PEG show that PVA-*g*-PEG and PVA exhibited cytotoxic effects in both cancerous cell lines HCT116 and SW620, resulting some alterations at the cell level. Fig. 9 shows that the increase in mortality is related to the increase of the AgNPs concentration in HCT116 and SW620 cell lines. A high mortality is obtained at high concentrations of PVA-*g*-PEG and PVA, while the mortality related to PEG did not exceed 20% for both HCT116 and SW620 cell lines. The 4PL regressions were used to the curves to determine the concentration at which 50% of the cells died in the presence of the polymers.[18]

PVA-*g*-PEG shows an IC50 of 25.42 ± 1.38 $\mu g\ mL^{-1}$ in HCT116 cells and 37.64 ± 2.07 $\mu g\ mL^{-1}$ in SW620 cells after 24 h for both, suggesting that the AgNPs prepared from PVA-*g*-PEG is a highly cytotoxic compound. PVA gives higher IC50 values of 51.15 ± 3.66 and 73.22 ± 4.87 $\mu g\ mL^{-1}$ in HCT116 and SW620 cell lines after 24 h, respectively, indicating that the AgNPs prepared from PVA is a moderately cytotoxic compound.[36–38] The lesser amount of PVA-*g*-PEG required comparing PVA to achieve 50% of mortality indicates the higher antineoplastic efficiency of PVA-*g*-PEG in both cell lines. Comparatively, the high IC50 values of 864.23 ± 5% and 1754.36 ± 5% $\mu g\ mL^{-1}$ obtained from PEG in HCT116 and SW620 cell lines, respectively, after 24 hours indicated that the AgNPs prepared from PEG exhibited no cytotoxicity against both cancerous cells without any antineoplastic properties. The standard deviations of IC50 in both cells were fixed to 5% due to large error ranges obtained. In terms of the selectivity of AgNPs/PVA-*g*-PEG, an evaluation of cellular viability with AgNPs/PVA-*g*-PEG was conducted in fibroblast cell lines (normal cells) to test potential cytotoxic effects in the noncancerous cells. The IC50 obtained with AgNPs/PVA-*g*-PEG in the normal cell was determined 165.74 ± 8.13 $\mu g\ mL^{-1}$ for 24 hours, suggesting a negligible toxicity in the normal cells.

## Conclusions

A grafted copolymer PVA-*g*-PEG comprising a PVA backbone and PEG branches was synthesized and used as a carrier to prepare the AgNPs/PVA-*g*-PEG composite in the presence of grape seeds extract. The AgNPs composites AgNPs/PVA and AgNPs/PEG which were prepared from homo-polymers were also synthesized using the same method to compare the antimicrobial and antitumor effect with that of AgNPs/PVA-*g*-PEG. Characterization of three AgNPs/polymer products indicated that the silver ions were successfully reduced by the grade seeds extract and the produced AgNPs are coated on the surface of AgNPs/PVA-*g*-PEG and AgNPs/PVA to form uniform and monodisperse nanoparticles with diameters of 25.7 ± 2.3 nm and 54.2 ± 3.4 nm, respectively. However, AgNPs/PEG formed only large aggregates. The good mono-dispersity and small size of AgNPs/

PVA-*g*-PEG could be attributed to the protective effect of PEG chain. The AgNPs/PVA-*g*-PEG and AgNPs/PVA composites exhibited excellent antimicrobial effects against *E. coli* and *S. aureus*. In addition, AgNPs/PVA-*g*-PEG had a better performance than AgNPs/PVA with an MIC of 1.3 μg $mL^{-1}$ and an MBC of 2.4 μg $mL^{-1}$. In terms of antitumor effect, AgNPs/PVA-*g*-PEG demonstrated a high cytotoxicity to the colorectal cancerous cells HCT116 and SW620. The IC50 values were determined 25.4 and 37.6 μg $mL^{-1}$ for HCT116 and SW620 cell lines, respectively. Therefore, AgNPs/PVA-*g*-PEG also possessed a better antitumor activity compared with AgNPs/PVA. Comparatively, the AgNPs/PEG did not exhibit significant antimicrobial and antitumor effects. This study has clearly demonstrated that the AgNPs/PVA-*g*-PEG composites have great potential applications in the control of microorganisms and inhibition of cancer cells.

## Data availability

The data supporting this article have been included in the figures of submitted manuscript.

## Conflicts of interest

There are no conflicts to declare.

## Acknowledgements

The authors acknowledge the financial support received from the National Natural Science Foundation of China (82102744), Applied Basic Research Program of Liaoning Province (2022JH2/101500011), China Post-Doctoral Science Foundation Grant (2023M744306), and Liaoning Provincial Science and Technology Plan – joint plan (2024JH2/102600273).

## References

1 A. Raghunath and E. Perumal, Metal Oxide Nanoparticles as Antimicrobial Agents: A Promise for the Future, *Int. J. Antimicrob. Agents*, 2017, **49**, 137–152.
2 V. Ramalingam, Silver Nanoparticles for Biomedical Applications, *Nanoparticle Ther. Prod. Technol. Types Nanoparticles, Regul. Asp.*, 2022, pp. 359–375.
3 P. R. More, S. Pandit, A. D. Filippis, G. Franci, I. Mijakovic and M. Galdiero, Silver Nanoparticles: Bactericidal and Mechanistic Approach against Drug Resistant Pathogens, *Microorganisms*, 2023, **11**, 369.
4 L. Wieler, O. Vittos, N. Mukherjee and S. Sarkar, Reduction in the COVID-19 Pneumonia Case Fatality Rate by Silver Nano particles: A Randomized Case Study, *Heliyon*, 2023, **9**, e14419.
5 C. A. Lopez-Ayuso, R. Garcia-Contreras, R. Manisekaran, M. Figueroa, M. C. Arenas-Arrocena, G. Hernandez-Padron, A. Pozos Guillén and L. S. Acosta-Torres, Evaluation of the Biological Responses of Silver Nanoparticles Synthesized Using Pelargonium x Hortorum Extract, *RSC Adv.*, 2023, **13**, 29784–29800.
6 P. Serrano-Díaz, D. W. Williams, J. Vega-Arreguin, R. Manisekaran, J. Twigg, D. Morse, R. García-Contreras, M. C. Arenas-Arrocena and L. S. Acosta-Torres, Geranium Leaf Mediated Synthesis of Silver Nanoparticles and Their Transcriptomic Effects on Candida Albicans, *Green Process. Synth.*, 2023, **12**, 20228105.
7 X. Gong, N. D. Jadhav, V. V. Lonikar, A. N. Kulkarni, H. Zhang, B. R. Sankapal, J. Ren, B. B. Xu, H. M. Pathan, Y. Ma, Z. Lin, E. Witherspoon, Z. Wang and Z. Guo, An Overview of Green Synthesized Silver Nanoparticles towards Bioactive Antibacterial, Antimicrobial and Antifungal Applications, *Adv. Colloid Interface Sci.*, 2024, **323**, 103053.
8 S. R. Kabir, H. Barabadi, E. Karimi and F. Sen, Editorial: Application of the Biogenic Silver Nanoparticles as Antimicrobial and Anticancer Agents, *Front. Chem.*, 2023, **11**, 1180027.
9 F. Arshad, G. A. Naikoo, I. U. Hassan, S. R. Chava, M. El Tanani, A. A. Aljabali and M. M. Tambuwala, Bioinspired and Green Synthesis of Silver Nanoparticles for Medical Applications: A Green Perspective, *Appl. Biochem. Biotechnol.*, 2023, **2023**, 1–34.
10 A. Panáček, L. Kvítek, R. Prucek, M. Kolář, R. Večeřová, N. Pizúrová, V. K. Sharma, T. Nevěčná and R. Zbořil, Silver Colloid Nanoparticles: Synthesis, Characterization, and Their Antibacterial Activity, *J. Phys. Chem. B*, 2006, **110**, 16248–16253.
11 F. Hakimian and M. Mazloum-Ardakani, Ag Nanorod@PEI-Ag Nanohybrid as an Excellent Signal Label for Sensitive and Rapid Detection of Serum HER2, *Sci. Rep.*, 2023, **13**, 1–11.
12 A. Menichetti, A. Mavridi-Printezi, D. Mordini and M. Montalti, Effect of Size, Shape and Surface Functionalization on the Antibacterial Activity of Silver Nanoparticles, *J. Funct. Biomater.*, 2023, **14**, 244.
13 A. A. Tayel, N. A. Elsayes, M. M. Zayed, M. A. Alsieni, F. A. Alatawi, A. I. Alalawy and A. M. Diab, Powerful Antibacterial Nanocomposites from Corallina Officinalis-Mediated Nanometals and Chitosan Nanoparticles against Fish-Borne Pathogens, *Green Process. Synth.*, 2023, **12**, 20230042.
14 Y. He, D. H. K. Ketagoda, R. Bright, S. M. Britza, J. Zechner, I. Musgrave, K. Vasilev and P. Zilm, Synthesis of Cationic Silver Nanoparticles with Highly Potent Properties against Oral Pathogens and Their Biofilms, *ChemNanoMat*, 2023, **9**, e202200472.
15 E. O. Uroro, R. Bright, P. R. L. Dabare, D. Bera, J. Y. Quek, N. Goswami and K. Vasilev, Biocompatible Polycationic Silver Nano cluster-Impregnated PLGA Nanocomposites with Potent Antimicrobial Activity, *ChemNanoMat*, 2022, **8**, e202200349.
16 S. Anees Ahmad, S. Sachi Das, A. Khatoon, M. Tahir Ansari, M. Afzal, M. Saquib Hasnain and A. Kumar Nayak, Bactericidal Activity of Silver Nanoparticles: A Mechanistic Review, *Mater. Sci. Energy Technol.*, 2020, **3**, 756–769.
17 D. A. M. Caltzonci, A. D. R. Chettiar, V. C. Ibarra, L. Marasamy, M. Loredo-Tovías, L. S. Acosta-Torres and

R. Manisekaran, Antimicrobial and Cytotoxic Effect of Positively Charged Nanosilver-Coated Silk Sutures, *ACS Omega*, 2024, **9**, 17636–17645.

18 L. M. Stabryla, P. J. Moncure, J. E. Millstone and L. M. Gilbertson, Particle-Driven Effects at the Bacteria Interface: A Nanosilver Investigation of Particle Shape and Dose Metric, *ACS Appl. Mater. Interfaces*, 2023, **15**, 39027–39038.

19 X. K. Hu, S. Cook, P. Wang and H. M. Hwang, In Vitro Evaluation of Cytotoxicity of Engineered Metal Oxide Nanoparticles, *Sci. Total Environ.*, 2009, **407**, 3070–3072.

20 N. Beyth, Y. Houri-Haddad, A. Domb, W. Khan and R. Hazan, Alternative Antimicrobial Approach: Nano-Antimicrobial Materials, *J. Evidence-Based Complementary Altern. Med.*, 2015, **2015**, 1–16.

21 H. D. Beyene, A. A. Werkneh, H. K. Bezabh and T. G. Ambaye, Synthesis paradigm and applications of silver nanoparticles (AgNPs), a review, *Sustainable Mater. Technol.*, 2017, **13**, 18–23.

22 L. J. Liu, C. A. Burnyeat, R. S. Lepsenyi, I. O. Nwabuko and T. L. Kelly, Mechanism of Shape Evolution in Ag Nanoprisms Stabilized by Thiol-Terminated Poly(Ethylene Glycol): An in Situ Kinetic Study, *Chem. Mater.*, 2013, **25**, 4206–4214.

23 V. Ravichandran, S. Vasanthi, S. Shalini, S. A. A. Shah and R. Harish, Green synthesis of silver nanoparticles using Atrocarpus altilis leaf extract and the study of their antimicrobial and antioxidant activity, *Mater. Lett.*, 2016, **180**, 264–267.

24 Q. Sun, X. Cai, J. Li, M. Zheng, Z. Chen and C. Yu, Green synthesis of silver nanoparticles using tea leaf extract and evaluation of their stability and antibacterial activity, *Colloids Surf., A*, 2014, **444**, 226–231.

25 J. Helmlinger, C. Sengstock, C. Groß-Heitfeld, C. Mayer, T. Schildhauer, M. Köller and M. Epple, Silver Nanoparticles with Different Size and Shape: Equal Cytotoxicity, but Different Antibacterial Effects, *RSC Adv.*, 2016, **6**, 18490–18501.

26 P. Van Dong, C. H. Ha, L. T. Binh and J. Kasbohm, Chemical Synthesis and Antibacterial Activity of Novel-Shaped Silver Nanoparticles, *Int. Nano Lett.*, 2012, **2**, 9.

27 M. Gao, L. Sun, Z. Wang and Y. Zhao, Controlled Synthesis of Ag Nanoparticles with Different Morphologies and Their Antibacterial Properties, *Mater. Sci. Eng., C*, 2013, **33**, 397–404.

28 M. Visnapuu, U. Joost, K. Juganson, K. Kunnis-Beres, A. Kahru, V. Kisand, *et al.*, Dissolution of Silver Nanowires and Nanospheres Dictates Their Toxicity to Escherichia Coli, *BioMed Res. Int.*, 2013, **2013**, 1–9.

29 M. Rojas-Andrade, A. T. Cho, P. Hu, S. J. Lee, C. P. Deming, S. W. Sweeney, *et al.*, Enhanced Antimicrobial Activity with Faceted Silver Nanostructures, *J. Mater. Sci.*, 2015, **50**, 2849–2858.

30 E. Ivanova, K. Bazaka and R. Crawford, Advanced Synthetic Polymer Biomaterials Derived from Organic Sources, *New Functional Biomaterials for Medicine and Healthcare*, ed. Ivanova, E. P., Bazaka, K. and Crawford, R. J., 2014, pp. 71–99.

31 D. Hu, X. Yang, W. Chen, Z. Feng, C. Hu, F. Yan, X. Chen, D. Qu and Z. Chen, Rhodiola rosea Rhizome Extract-Mediated Green Synthesis of Silver Nanoparticles and Evaluation of Their Potential Antioxidant and Catalytic Reduction Activities, *ACS Omega*, 2021, **6**, 24450–24461.

32 M. Liang, R. Su, R. Huang, W. Qi, Y. Yu, L. Wang and Z. He, Facile in Situ Synthesis of Silver Nanoparticles on Procyanidin-Grafted Eggshell Membrane and Their Catalytic Properties, *ACS Appl. Mater. Interfaces*, 2014, **6**, 4638–4649.

33 R. Mitra, P. Figueroa, A. K. Mukhopadhyay, T. Shimada, Y. Takeda, D. E. Berg and G. B. Nair, Cell Vacuolation, a Manifestation of the El Tor Hemolysin of Vibrio Cholerae, *Infect. Immun.*, 2000, **68**, 1928–1933.

34 M. Özyürek, N. Güngör, S. Baki, K. Güçlü and R. Apak, Development of a Silver Nanoparticle-Based Method for the Antioxidant Capacity Measurement of Polyphenols, *Anal. Chem.*, 2012, **84**, 8052–8059.

35 E. Tamariz and F. Grinnell, Modulation of Fibroblast Morphology and Adhesion during Collagen Matrix Remodeling, *Mol. Biol. Cell*, 2002, **13**, 3915–3929.

36 T. A. Loomis and A. W. Hayes, *Loomi's Essentials of Toxicology*, Academic Press, California, 4th edn, 1996, pp 208–245.

37 P. W. Prasetyaningrum, A. Bahtiar and H. Hayun, Synhtesis and Cytotoxicity Evaluation of Novel Asymmetrical Mono-Carbonyl Analogs of Curcumin (AMACs) against Vero, HeLa, and MCF7 Cell Lines, *Sci. Pharm.*, 2018, **86**, 25.

38 Q. Q. Li, G. Wang, E. Reed, L. Huang and C. F. Cuff, Evaluation of Cisplatin in Combination with β-Elemene as a Regimen for Prostate Cancer Chemotherapy, *Basic Clin. Pharmacol. Toxicol.*, 2010, **107**, 868–876.

39 S. Karmakar, I. Poetsch, C. R. Kowol, P. Heffeter and D. Gibson, Synthesis and Cytotoxicity of Water-Soluble Dual- and Triple-Action Satraplatin Derivates: Replacement of Equatorial Chlorides of Satraplatin by Acetates, *Inorg. Chem.*, 2019, **58**, 16676–16688.

40 S. Narayanan, B. N. Sathy, U. Mony, M. Koyakutty, S. V. Nair and D. Menon, Biocompatible Magnetite/Gold Nanohybrid Contrast Agents via Green Chemistry for MRI and CT Bioimaging, *ACS Appl. Mater. Interfaces*, 2012, **4**, 251–260.

41 D. Bagchi, M. Bagchi, S. J. Stohs, D. K. Das, S. D. Ray, C. A. Kuszynski, S. S. Joshi and H. G. Pruess, Free radicals and grape seed proanthocyanidin extract: importance in human health and disease prevention, *Toxicology*, 2000, **148**, 187–197.

42 G. Paradossi, F. Cavalieri, E. Chiessi, C. Spagnoli and M. K. Cowman, Poly(vinyl alcohol) as versatile biomaterial for potential biomedical applications, *J. Mater. Sci.: Mater. Med.*, 2003, **14**, 687–691.

43 A. B. Salunkhe, V. M. Khot, N. D. Thorat, M. R. Phadatare, C. I. Sathish, D. S. Dhawale and S. H. Pawar, Polyvinyl alcohol functionalized cobalt ferrite nanoparticles for biomedical applications, *Appl. Surf. Sci.*, 2013, **264**, 598–604.

44 N. Georgieva, R. Bryaskova and R. Tzoneva, New Polyvinyl alcohol-based hybrid materials for biomedical application, *Mater. Lett.*, 2012, **88**, 19–22.
45 A. Abdelfattah, A. E. Aboutaleb, A. B. M. Abdel-Aal, A. A. H. Abdellatif, H. M. Tawfeek and S. I. Abdel-Rahman, Design and optimization of PEGylated silver nanoparticles for efficient delivery of doxorubicin to cancer cells, *J. Drug Delivery Sci. Technol.*, 2022, **71**, 103347.
46 O. J. Oziri, B. Wang, T. Watanabe, S. Uno, M. Maeki, M. Tokeshi, T. Isono, K. Tajima, T. Satoh, S. Sato, Y. Miura and T. Yamamoto, PEGylation of silver nanoparticles by physisorption of cyclic poly(ethylene glycol) for enhanced dispersion stability, antimicrobial activity, and cytotoxicity, *Nanoscale Adv.*, 2022, **4**, 532–545.
47 K. Li, C. Ma, T. Jian, H. Sun, L. Wang, H. Xu, W. Li, H. Su and X. Cheng, Making good use of the byproducts of cultivation: green synthesis and antibacterial effects of silver nanoparticles using the leaf extract of blueberry, *J. Food Sci. Technol.*, 2017, **54**, 3569–3576.
48 C. Z. Chen and S. L. Cooper, Interactions between dendrimer biocides and bacterial membranes, *Biomaterials*, 2002, **23**, 3359–3368.
49 S. Chen, J. Duhamel and M. A. Winnik, Probing End-to-End Cyclization beyond Willemski and Fixman, *J. Phys. Chem. B*, 2011, **115**, 3289–3302.
50 J. M. Dust, Z. H. Fang and J. M. Harris, Proton NMR characterization of poly(ethylene glycols) and derivatives, *Macromolecules*, 1990, **23**, 3742–3746.
51 B. Sadeghi and F. Gholamhoseinpoor, A study on the stability and green synthesis of silver nanoparticles using Ziziphora tenuior (Zt) extract at room temperature, *Spectrochim. Acta, Part A*, 2015, **134**, 310–315.
52 M. Darroudi, M. B. Ahmad and M. Mashreghi, Gelatinous silver colloid nanoparticles: Synthesis, characterization, and their antibacterial activity, *J. Optoelectron. Adv. Mater.*, 2014, **16**, 182–187.
53 G. A. Sotiriou and S. E. Pratsinis, Antibacterial activity of nanosilver ions and particles, *Environ. Sci. Technol.*, 2010, **44**, 5649–5654.
54 H. A. Widatalla, L. F. Yassin, A. A. Alrasheid, S. A. R. Ahmed, M. S. Widdatallah, S. H. Eltilib and A. A. Mohamed, Green synthesis of silver nanoparticles using green tea leaf extract, characterization and evaluation of antimicrobial activity, *Nanoscale Adv.*, 2022, **4**, 911–915.
55 P. K. Khanna, N. Singh, S. Charan, V. V. V. S. Subbarao, R. Gokhale and U. P. Mulik, Synthesis and characterization of Ag/PVA nanocomposite by chemical reduction method, *Mater. Chem. Phys.*, 2005, **93**, 117–121.
56 M. Mostafa, H. E. Ramadan and M. A. El-Amir, Sorption and desorption studies of radioiodine onto silver chloride via batch equilibration with its aqueous media, *J. Environ. Radioact.*, 2015, **150**, 9–19.
57 G. Gahlawat, S. Shikha, B. S. Chaddha, S. R. Chaudhuri, S. Mayilraj and A. R. Choudhury, Microbial glycolipoprotein-capped silver nanoparticles as emerging antibacterial agents against cholera, *Microb. Cell Fact.*, 2016, **15**, 25.
58 Q. L. Feng, J. Wu, G. Q. Chen, F. Z. Cui, T. N. Kim and J. O. Kim, A mechanistic study of the antibacterial effect of silver ions on Escherichia coli and Staphylococcus aureus, *J. Biomed. Mater. Res.*, 2000, **52**, 662–668.
59 W. Li, X. Xie, Q. Shi, H. Zeng, Y. S. Ou-Yang and Y. Chen, Antibacterial activity and mechanism of silver nanoparticles on Escherichia coli, *Appl. Microbiol. Biotechnol.*, 2010, **85**, 1115–1122.
60 S. Shen, T. Zhang, Y. Yuan, S. Lin, J. Xu and H. Ye, Effects of cinnamaldehyde on Escherichia coli and Staphylococcus aureus membrane, *Food Control*, 2015, **47**, 196–202.